Journal of Alloys and Compounds 766 (2018) 511–516

Contents lists available at ScienceDirect

Journal of Alloys and Compounds

journal homepage: http://www.elsevier.com/locate/jalcom

ω-phase transformation and lattice modulation in biomedical β-phase Ti-Nb-Al alloys

Pan Wang [a, b, *], Mitsuharu Todai [a], Takayoshi Nakano [a, **]

[a] Division of Materials and Manufacturing Science, Graduate School of Engineering, Osaka University, Suita, Osaka 565-0871, Japan
[b] Singapore Institute of Manufacturing Technology, 73 Nanyang Drive, 637662, Singapore

ARTICLE INFO

Article history:
Received 4 May 2018
Received in revised form
21 June 2018
Accepted 23 June 2018
Available online 28 June 2018

Keywords:
β-Ti alloy
Biomaterials
Electronic properties
Microstructure
Phase transitions
Transmission electron microscopy (TEM)

ABSTRACT

Athermal ω-phase transformation and the appearance of the lattice modulation in Ti-28Nb-*x*Al alloys were investigated by electrical resistivity measurements and transmission electron microscopy (TEM) observations. As a result, the athermal ω-phase is gradually suppressed with increasing Al content. In addition, the lattice modulation is also observed in Ti-28Nb-*x*Al alloys ($0 \leq x \leq 7$, in at.%) because of the transverse wave with a propagation vector of $\boldsymbol{q} = 1/2[\zeta\bar{\zeta}0]^*$ and displacement in [110]. These results imply that the ω-phase can be controlled by addition of the Al content in Ti-Nb alloys, leading to the development of low Young's modulus β-phase Ti biomedical alloys single crystal.

1. Introduction

Ti and Ti alloys are widely used as biomaterials because they possess good biocompatibility, superior strength and excellent corrosion resistance. In particular, β-phase Ti alloys with body-centered cubic structures have attracted considerable attention as hard tissue because β-phase Ti alloys exhibit low Young's modulus [1,2]. It is necessary for the prevention of bone degradation and absorption caused by the gap of Young's modulus between the replacements and natural human bone, which is the so-called stress shielding [2–5]. Thus, many studies have been conducted to give the low Young's modulus and appropriate plastic deformation behavior of some β-phase Ti alloys [6–15].

Recently, our group investigated the elastic stiffness and elastic anisotropy of Ti-Nb-Ta-Zr alloy and Ti-Mo-Zr-Al alloy using their single crystals [10,13,16]. It is found that the Young's modulus along the <001> direction in β-phase Ti single crystals with low *e*/*a* ratio is similar to that of human bone and is the lowest in all crystallographic orientations. The *e*/*a* is the average number of valence electron per atom in the free atom configuration. In addition, it is proposed that suppressing of the formation of ω-phase and decreasing *e*/*a* ratio are important criteria for reducing the Young's modulus of β-phase Ti single crystals [13]. Reduction of the Young's modulus of β-phase Ti single crystals is caused by the lattice softening corresponding to low elastic stiffness, c'. Zener has insisted that the value of c' indicates the β-phase stability [17]. Moreover, we also reported that the lattice softening and low β-phase stability in Ti-Nb alloys are also closely related to the lattice modulation [18]. This lattice modulation, exhibits nanodomains morphology, is caused by a transverse wave in some β Ti-Nb alloys with low *e*/*a*, such as (Ti-23Nb)-1.0O alloy [19] and Ti-Nb alloys [20]. However, the athermal ω-phase that increases the Young's modulus dramatically [6,7,9,18–20,28] always easy to present in the low β-phase stability Ti alloys accompanied by lattice modulation [18–20,28]. Based on these viewpoints, it is very important to suppress athermal ω-phase and remain the β-phase with lattice modulation even in Ti-Nb base alloy with low *e*/*a*. The transformation behavior and phase constitution were investigated in the binary Ti-Nb alloy. The athermal ω-phase appears in the Ti-28Nb (in at.%) alloy but is suppressed in Ti-30Nb alloy which exhibits low *e*/*a*, a lattice modulation and a low Young's modulus [18,21]. Thus, it can be expected that the suppression of the athermal ω-

* Corresponding author. Division of Materials and Manufacturing Science, Graduate School of Engineering, Osaka University, Suita, Osaka 565-0871, Japan.
** Corresponding author.
E-mail addresses: wangp@SIMTech.a-star.edu.sg (P. Wang), nakano@mat.eng.osaka-u.ac.jp (T. Nakano).

https://doi.org/10.1016/j.jallcom.2018.06.266

phase in Ti-28Nb leads to the reduction of the Young's modulus. Therefore, the purpose of the present study is to clarify the ω-phase transformation and appearance of the lattice modulation in Ti-28Nb-*x*Al alloy because it is known that additional of Al element into some Ti alloys caused suppression of the athermal ω-phase and thermal ω-phase [13].

2. Experimental procedure

Ingots of Ti-28Nb-*x*Al alloys ($x = 0$, 1, 3, 5 and 7 in at. %) were prepared by an arc melting method. They were subject to homogenized heat treatment at 1273 K, 24 h under high purity Ar gas. Afterward, specimens for all measurements were cut from these ingots and subsequently solution treated at 1173 K for 1 h and then quenched into ice water. Table 1 shows the analyzed chemical compositions and the *e*/*a* of the Ti-28Nb-*x*Al alloys. The *e*/*a* was calculated using the analyzed chemical compositions of Ti, Nb and Al on the basis of the electron configurations Ti ($[Ar]3d^2 4s^2$), Nb ($[Kr]4d^4 5s^1$) and Al ($[Ne]3d^2 3p^1$). Each alloy is hereinafter referred to by its Al content, e.g., Ti-28Nb-7Al is represented by 7Al. The oxidized surface layer was removed using electropolishing in a solution of 6 vol% perchloric acid, 35 vol% butanol and 59 vol% methanol at about 230 K. Electrical resistivity was measured using a standard four probe method with a current of 200 mA and a frequency of 10 Hz. The cooling and heating rate is 1 K/min. XRD measurements were conducted at room temperature with Cu Kα radiation. Thin foils for TEM observation were prepared using electropolishing in an acidic electrolyte. TEM observation was performed using a JEM 3010 operated at 300 kV at room temperature and a HITACHI H-800 equipped with a liquid N_2 cooling stage and operated at 200 kV at low temperature. The specimens for low-temperature observation were cooled to about 90 K and then heated to various temperatures below room temperature.

3. Results and discussion

3.1. XRD measurements

In order to confirm the phase constitutions, XRD measurements were carried out. Fig. 1 shows the XRD patterns of Ti-28Nb-*x*Al ($0 \le x \le 7$) alloys. Only the β-phase was detected at room temperature. In the previous study, we reported the precipitation of athermal ω-phase in 0Al alloy at room temperature by TEM observation [18]. It is reasonable that the small volume fraction of the athermal ω-phase contained in these alloys was insufficient to be detected by XRD [15]. On the other hand, the peak of β-phase shifted to a higher angle. This means that β-phase lattice parameters decrease with increasing Al content because the atomic radius of Al (1.43 Å) is smaller than Ti (1.47 Å).

3.2. Electrical resistivity measurements

The variation of the electrical resistivity curves of the Ti-28Nb-*x*Al ($0 \le x \le 7$) alloys is shown in Fig. 2(a). The graphs for the resistivity curves of the Ti-28Nb-*x*Al alloys ($0 \le x \le 5$) during cooling process exhibits a local minimum, T_{min}, as indicated by an arrow. The graph of 0Al alloy is in good agreement with previous studies [18,20]. An anomalous negative temperature coefficient (NTC) was observed below T_{min} in these alloys. This NTC is also observed in some β-phase Ti alloys [20,22–25] and is interpreted as the growth of the athermal ω-phase and the appearance of lattice modulation [20]. After the increase, the resistivity of these alloys decreases again at a local maximum, T_{max}, as indicated with double arrows. A small thermal hysteresis (~3 K) was also observed between cooling and heating processes and could be related to the athermal ω-phase transformation because this transformation is the first order transformation [20,25]. Fig. 2(b) shows the composition dependence of the T_{min} and T_{max}. These values decreased with increasing Al content. On the other hand, the resistivity of 7Al alloy exhibited neither an NTC nor thermal hysteresis in the measured temperature range, these results imply that the athermal ω-phase could be gradually suppressed with increasing Al content. Moreover, the 7Al alloy showed temperature independence of electrical resistivity between 60 K and 130 K. This resistivity curve exhibits a similar shape to that of the Ti-30Nb alloy which exhibits lattice modulation and low Young's modulus [18,20,21]. Incidentally, the abrupt decrease in resistivity curve below 10 K observed for all the alloys was due to a superconducting transition. The superconducting transition temperature, T_c, of all specimens monotonically decreased with increasing Al content as shown in Fig. 3.

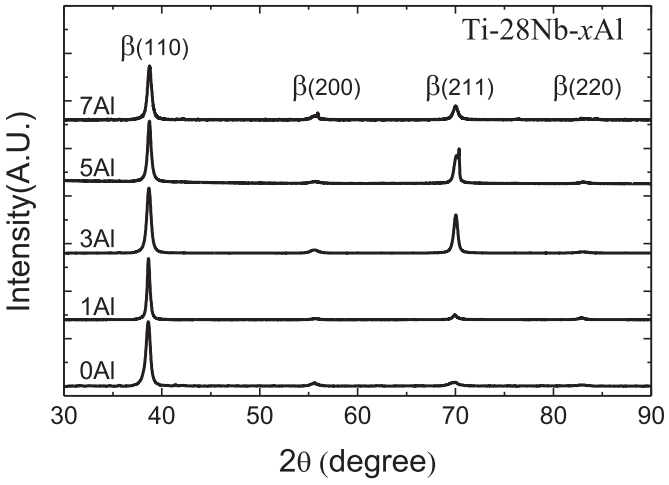

Fig. 1. XRD patterns of Ti-28Nb-*x*Al ($0 \le x \le 7$) alloys at room temperature.

3.3. TEM observations at room temperature

Fig. 4 shows the bright-field images and the typical selected area diffraction patterns (SADPs) taken with a beam direction of [113] of the Ti-28Nb-*x*Al ($x = 1, 3, 5, 7$) at room temperature, respectively. It is noted that flat microstructure appeared and self-accommodated structure which was caused by martensitic transformation was not observed in all the examined alloys as shown in Fig. 4(a–d). Fig. 4(a′) shows the diffraction pattern of the β-phase, additional slight streaks along the $<112>^*$ direction and diffuse satellites at $\boldsymbol{g}_\beta + 1/3<\zeta\zeta 2\zeta>^*$ and $\boldsymbol{g}_\beta + 2/3<\zeta\zeta 2\zeta>^*$, where the asterisk (*) implies orientation in a reciprocal lattice space and $\boldsymbol{g}_\beta$ is the β-phase reciprocal lattice vector. These satellites are characteristic to the ω-phase [26,27]. The diffuse satellites of the ω-phase were also observed at $\boldsymbol{g}_\beta + 1/3<\zeta\zeta\zeta>^*$ and $\boldsymbol{g}_\beta + 2/3<\zeta\zeta\zeta>^*$ when a beam direction was [110], as shown in Fig. 5(a). The appearance of these

Table 1
Chemical compositions of solution treated Ti-28Nb-*x*Al alloys in at. % units, and corresponding *e*/*a* ratios.

	Ti	Nb	Al	*e*/*a*
(at.%)				
Ti-28Nb	Bal.	27.92	0	4.28
Ti-28Nb-1Al	Bal.	28.05	1.10	4.27
Ti-28Nb-3Al	Bal.	28.07	3.08	4.25
Ti-28Nb-5Al	Bal.	27.80	5.07	4.23
Ti-28Nb-7Al	Bal.	28.07	7.06	4.21

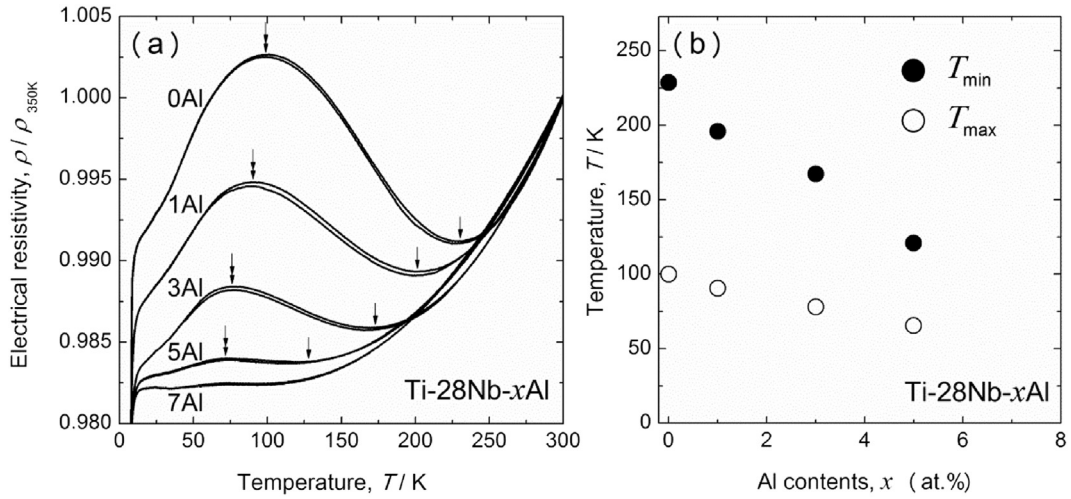

Fig. 2. (a) Temperature dependence of electrical resistivity of Ti-28Nb-*x*Al ($0 \le x \le 7$) alloys [18] and (b) aluminum content dependence of T_{min} and T_{max}.

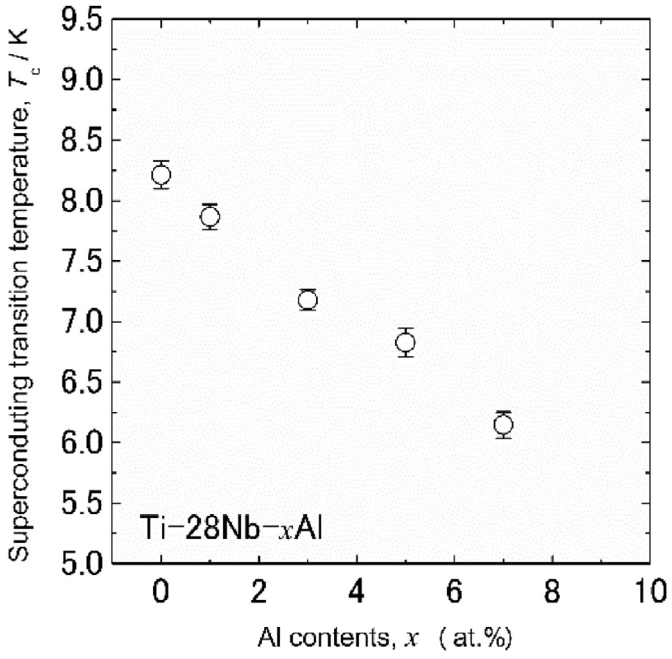

Fig. 3. Aluminum content dependence of superconducting transition temperature, T_c, for Ti-28Nb-*x*Al ($0 \le x \le 7$) alloys.

satellites in the 1Al alloy can be seen more clearly by one-dimensional line profile as shown in Fig. 6. From these results, athermal ω-phase appeared in the 1Al alloy at room temperature. The intensity of diffuse satellites of the ω-phase diffuse satellites decreased with increasing Al content. These diffuse satellites cannot be observed in the 7Al alloy. The disappearance of diffuse satellites of the ω-phase can be seen more clearly by comparing the line profiles of 1Al alloy in Fig. 6. Thus, the athermal ω-phase was gradually suppressed by addition of Al content. In addition, it was also observed the streaks along $[1\bar{1}0]^*$ and diffuse satellites at $\boldsymbol{g}_\beta + 1/2[1\bar{1}0]^*$ which was very weak and indicated by arrows in Fig. 4(a′). It is expected that these are caused by the transverse lattice modulation [19,20,28]. To confirm the appearance of the transverse lattice modulation, we observed the streaks along the $[1\bar{1}0]^*$ and diffuse satellites at $\boldsymbol{g}_\beta + 1/2[\zeta\bar{\zeta}0]^*$ in the different SADPs of the 3Al alloy. Fig. 7(a) shows the diffraction pattern with a beam direction of [001], and Fig. 7(b) shows the diffraction pattern when the specimen is tilted by approximately 5° from its position in Fig. 7(a). It can be observed the disappearance of the streaks along $[1\bar{1}0]^*$ and diffuse satellites at $\pm 1/2[1\bar{1}0]^*$. This appearance of streaks and satellites implies that streaks and satellites appear due to double diffraction [29,30]. Thus, the transverse lattice modulation also exists in the Ti-28Nb-*x*Al alloys. In addition, it can be seen that these streaks and diffuse satellites appeared in the SADPs with a beam direction is [113] and [001], but not [110], as shown in Figs. 4 and 5. These results imply that the satellites diffraction are missing in the case when the inner product of the scattering vector of these diffraction $\boldsymbol{g}$ and the displacement of atoms $\boldsymbol{R}$ is zero. Where, $\boldsymbol{g} = \boldsymbol{g}_\beta + \boldsymbol{q}$. $\boldsymbol{q}$ is the propagation vector for the displacement of atoms $\boldsymbol{R}$. In addition, $\boldsymbol{q}\cdot\boldsymbol{R}$ is always zero because the $\boldsymbol{R}$ is given by transverse wave. Therefore, the equation of $\boldsymbol{g}\cdot\boldsymbol{R} = 0$ is satisfied only when $\boldsymbol{g}_\beta \cdot \boldsymbol{R} = 0$ and leads to missing the diffuse satellites at $\boldsymbol{g}_\beta + 1/2[\zeta\bar{\zeta}0]^*$ in SADPs with a beam direction is [110]. These results further imply that the satellites at $\boldsymbol{g}_\beta + 1/2[\zeta\bar{\zeta}0]^*$ appear because of a transverse wave consistent with the displacement of atoms in the [110] direction, which is perpendicular to the propagation vector $\boldsymbol{q} = 1/2<\zeta\bar{\zeta}0>^*$. It is reported that the same lattice modulation is also observed in the Ti-Nb alloys and Ti-Nb-O alloys with low *e*/*a* [18–20,28]. The intensity of the satellites at $\boldsymbol{g}_\beta + 1/2[\zeta\bar{\zeta}0]^*$ presumably has a temperature dependence and increases below T_{min} as in Ti-Nb binary alloys [20].

3.4. In-situ TEM observations at low temperature

To confirm the suppression of athermal ω-phase and temperature dependence lattice modulation in the 7Al alloy, *in-situ* TEM observations were carried out below room temperature. Fig. 8(a–d) show the SADPs of the 7Al single crystal taken with a beam direction of [113] at 100 K, 150 K, 200 K and 275 K, respectively. The intensity of diffuse satellites at $\boldsymbol{g}_\beta + 1/3<\zeta\zeta 2\zeta>^*$ and $\boldsymbol{g}_\beta + 2/3<\zeta\zeta 2\zeta>^*$ related athermal ω-phase cannot be observed. The detailed intensity of these diffuse satellites was investigated by the one-dimensional intensity profile measured along the dotted line as shown in Fig. 8(a) and the results are shown in Fig. 8(e). It is evident from the line profiles that no distinct diffuse satellites at $\boldsymbol{g}_\beta + 1/3<\zeta\zeta 2\zeta>^*$ and $\boldsymbol{g}_\beta + 2/3<\zeta\zeta 2\zeta>^*$ appears. It is implied that the athermal ω-phase is completely suppressed in the 7Al alloy at low temperatures. Fig. 9(a–d) show the SADPs of 7Al alloy taken with a beam direction of [001] at 100 K, 150 K, 200 K and 250 K,

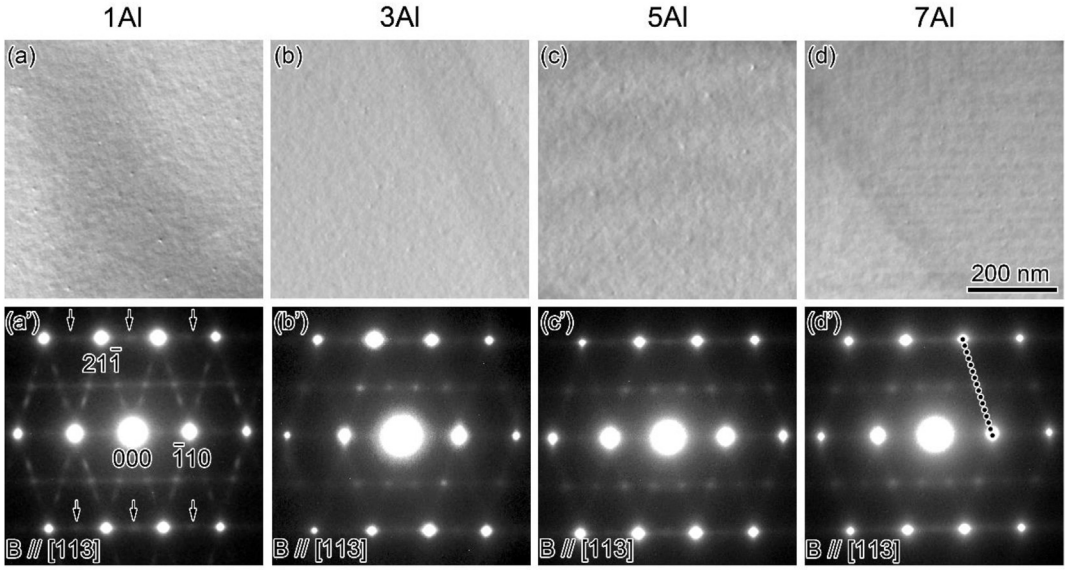

Fig. 4. Variations in (a–d) bright-field image and (a′-d') corresponding SADPs with beam direction is $[113]_\beta$ of Ti-28Nb-*x*Al ($1 \leq x \leq 7$) alloys at room temperature. (a and a′) 1Al; (b and b′) 3Al; (c and c′) 5Al; and (d and d′) 7Al.

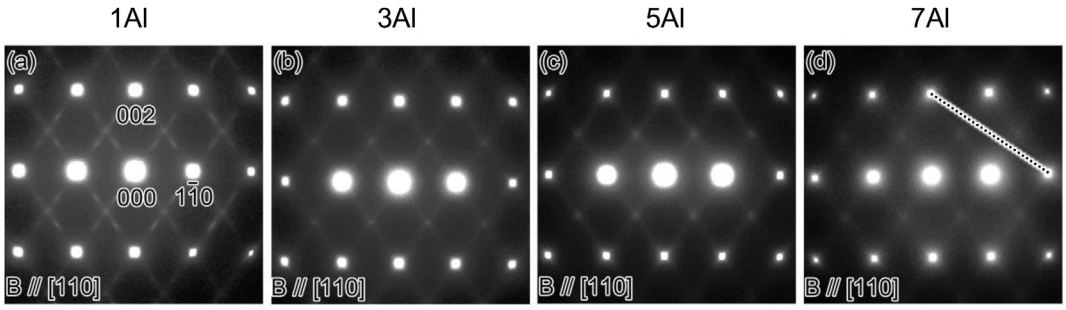

Fig. 5. Variations in SADPs with beam direction is $[110]_\beta$ in the (a) 1Al; (b) 3Al; (c) 5Al; and (d) 7Al alloys at room temperature.

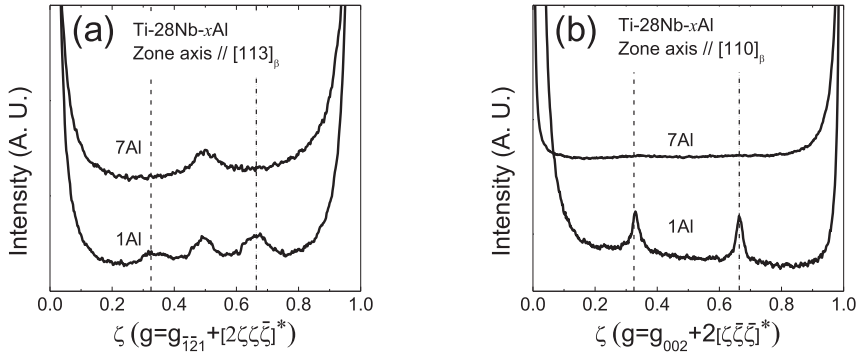

Fig. 6. One-dimensional intensity profile from (a) $[2\zeta\zeta\bar{\zeta}]^*$ direction in Fig. 4 (d′) and (b) $2[\zeta\zeta\bar{\zeta}]^*$ in Fig. 5(d) of the 1Al and 7Al alloys.

respectively. The intensity of diffuse satellites at $\boldsymbol{g}_\beta + 1/2<\zeta\bar{\zeta}0>^*$ position related lattice modulation was observed. Fig. 9(e) shows the intensity profiles along the $[\zeta\bar{\zeta}0]^*$ direction, as indicated by the dotted line in Fig. 9(a). The intensity of diffuse satellites at $\boldsymbol{g}_\beta + 1/2<\zeta\bar{\zeta}0>^*$ position slightly increased with decreasing temperature. It is suggested that the lattice modulation shows clear temperature dependence with decreasing temperature and possibly is related to the bend on resistivity curve. The formation and growth of lattice modulation imply a lattice perturbation, and consequently, makes the resistivity increase. Therefore, an increase of the resistivity with the formation of lattice modulation was observed, which caused the bend of resistivity curve after the formation of lattice modulation.

As described above, it can be controlled the appearing of ω-phase by addition of the Al content in Ti-Nb alloys. Athermal ω-phase was suppressed at the same time lattice modulation was retained in the 7Al alloy with low *e*/*a*. Consequently, it is expected that the 7Al alloy single crystal exhibits the low Young's modulus

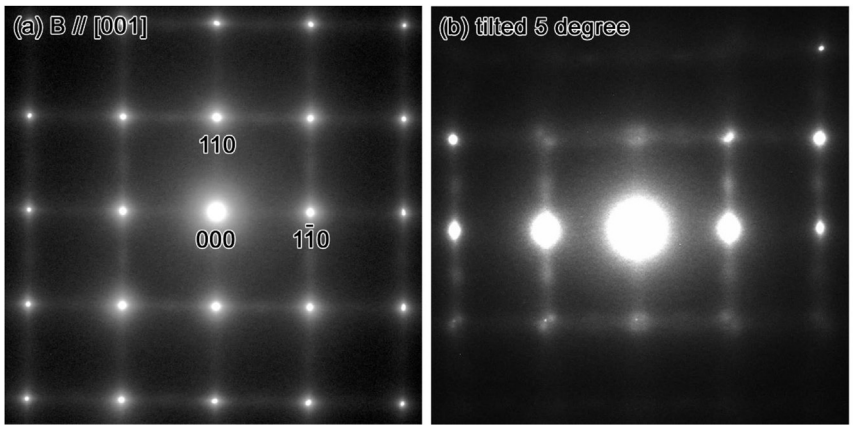

Fig. 7. SADPs in the 3Al alloy at room temperature. (a) beam direction is $[001]_\beta$ and (b) is for the systematic condition.

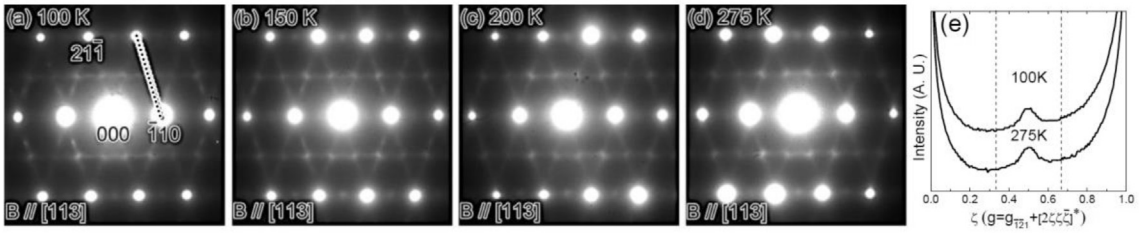

Fig. 8. SADPs generated at low temperature for the 7Al alloy in the beam direction of $[113]_\beta$. (a)100 K; (b) 150 K; (c) 200 K; (d) 275 K and (e) intensity profiles from $[2\zeta\zeta\bar{\zeta}]^*$ direction.

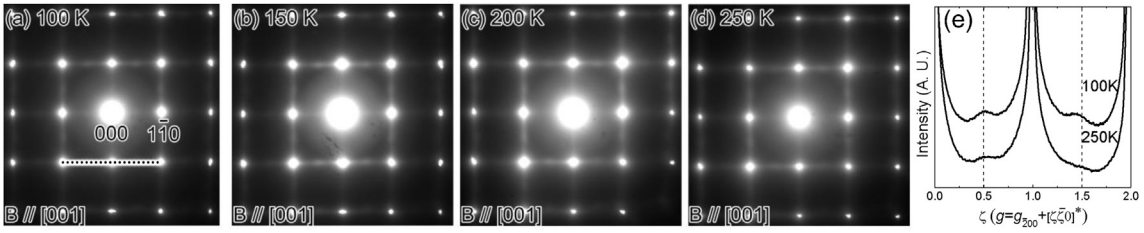

Fig. 9. SADPs generated at low temperature for the 7Al alloy in the beam direction of $[001]_\beta$. (a)100 K; (b) 150 K; (c) 200 K; (d) 250 K and (e) intensity profiles from $[\zeta\bar{\zeta}0]^*$ direction.

along <001>, which is caused by the lattice softening of c' in instability β-phase with lattice modulation. To develop the single crystalline of β-phase Ti alloy implant with an extremely low Young's modulus, the 7Al alloy is one of the promising candidates for biomaterials. The single crystal of the 7Al alloy has been grown and further study to reveal the Young's modulus using its single crystal is now in progress.

4. Conclusions

The appearance of the ω-phase and the lattice modulation in Ti-Nb-*x*Al ($0 \leq x \leq 7$ in at. %) alloys were investigated by electrical resistivity measurements and TEM observations. The results were summarized as follows:

(1) Ti-28Nb-*x*Al ($0 \leq x \leq 5$) alloys exhibited an NTC and a thermal hysteresis in the electrical resistivity curve related to athermal ω-phase precipitation and lattice modulation in β-phase. On the other hand, the 7Al alloy did not exhibit an NTC and a thermal hysteresis.
(2) Athermal ω-phase was gradually suppressed with increasing Al content and was completely suppressed in the 7Al alloy.
(3) The lattice modulation appeared in Ti-28Nb-*x*Al ($0 \leq x \leq 7$) alloys and also had a propagation vector of $\boldsymbol{q} = 1/2[\zeta\bar{\zeta}0]^*$ and displacement in [110] appears. This lattice modulation presented temperature dependence and was related to the bend on resistivity curve.

Acknowledgments

This work was supported by the Funding Program for Next Generation World-Leading Researchers from the Japan Society for the Promotion of Science (JSPS), the Ministry of Education, Culture, Sports, Science, Technology (MEXT) of Japan and by the Grants-in-Aid for Scientific Research (S) and Young Scientists (B) from the Japan Society for Promotion of Science (JSPS) and a research grant from the Light Metal Educational Foundation.

References

[1] M. Geetha, A. Singh, R. Asokamani, A. Gogia, Ti based biomaterials, the ultimate choice for orthopaedic implants–A review, Prog. Mater. Sci. 54 (2009) 397–425.
[2] D. Banerjee, J.C. Williams, Perspectives on titanium science and Technology, Acta Mater. 61 (2013) 844–879.

[3] Y. Noyama, T. Nakano, T. Ishimoto, T. Sakai, H. Yoshikawa, Design and optimization of the oriented groove on the hip implant surface to promote bone microstructure integrity, Bone 52 (2013) 659–667.
[4] M. Niinomi, Recent research and development in titanium alloys for biomedical applications and healthcare goods, Sci. Technol. Adv. Mater. 4 (2003) 445–454.
[5] A. Matsugaki, G. Aramoto, T. Nakano, The alignment of MC3T3-E1 osteoblasts on steps of slip traces introduced by dislocation motion, Biomaterials 33 (2012) 7327–7335.
[6] P. Wang, Y. Feng, F. Liu, L. Wu, S. Guan, Microstructure and mechanical properties of Ti–Zr–Cr biomedical alloys, Mater. Sci. Eng. C 51 (2015) 148–152.
[7] T. Ozaki, H. Matsumoto, S. Watanabe, S. Hanada, Beta Ti alloys with low Young's modulus, Mater. Trans. 45 (2004) 2776–2779.
[8] L.A. Matlakhova, A.N. Matlakhov, S.N. Monteiro, S.G. Fedotov, B.A. Goncharenko, Properties and structural characteristics of Ti–Nb–Al alloys, Mater. Sci. Eng. A 393 (2005) 320–326.
[9] P. Wang, L. Wu, Y. Feng, J. Bai, B. Zhang, J. Song, S. Guan, Microstructure and mechanical properties of a newly developed low Young's modulus Ti–15Zr–5Cr–2Al biomedical alloy, Mater. Sci. Eng. C 72 (2017) 536–542.
[10] M. Tane, S. Akita, T. Nakano, K. Hagihara, Y. Umakoshi, M. Niinomi, H. Nakajima, Peculiar elastic behavior of Ti-Nb-Ta-Zr single crystals, Acta Mater. 56 (2008) 2856–2863.
[11] T. Inamura, Y. Yamamoto, H. Hosoda, H.Y. Kim, S. Miyazaki, Crystallographic orientation and stress-amplitude dependence of damping in the martensite phase in textured Ti-Nb-Al shape memory alloy, Acta Mater. 58 (2010) 2535–2544.
[12] Y. Zhang, S. Li, E. Obbard, H. Wang, S. Wang, Y. Hao, R. Yang, Elastic properties of Ti–24Nb–4Zr–8Sn single crystals with bcc crystal structure, Acta Mater. 59 (2011) 3081–3090.
[13] S.H. Lee, M. Todai, M. Tane, K. Hagihara, H. Nakajima, T. Nakano, Biocompatible low Young's modulus achieved by strong crystallographic elastic anisotropy in Ti-15Mo-5Zr-3Al alloy single crystal, J. Mech. Behav. Biomed. Mater. 14 (2012) 48–54.
[14] S.-H. Lee, K. Hagihara, T. Nakano, Microstructural and orientation dependence of the plastic deformation behavior in β-type Ti-15Mo-5Zr-3Al alloy single crystals, Metall. Mater. Trans. A (2012) 1–10.
[15] X. Zhao, M. Niinomi, M. Nakai, J. Hieda, Beta type Ti–Mo alloys with changeable Young's modulus for spinal fixation applications, Acta Biomater. 8 (2012) 1990–1997.
[16] M. Tane, S. Akita, T. Nakano, K. Hagihara, Y. Umakoshi, M. Niinomi, H. Mori, H. Nakajima, Low Young's modulus of Ti-Nb-Ta-Zr alloys caused by softening in shear moduli c' and c_{44} near lower limit of body-centered cubic phase stability, Acta Mater. 58 (2010) 6790–6798.
[17] C. Zener, Contributions to the theory of beta-phase alloys, Phys. Rev. 71 (1947) 846–851.
[18] P. Wang, M. Todai, T. Nakano, β-phase instability in binary Ti-xNb biomaterial single crystals, Mater. Trans. 54 (2013) 156–160.
[19] M. Tahara, H.Y. Kim, T. Inamura, H. Hosoda, S. Miyazaki, Lattice modulation and superelasticity in oxygen-added β-Ti alloys, Acta Mater. 59 (2011) 6208–6218.
[20] M. Todai, T. Fukuda, T. Kakeshita, Relation between negative temperature coefficient in electrical resistivity and athermal ω phase in Ti–xNb ($26 \leq x \leq 29$ at.%) alloys, J. Alloys Compd. 577 (2013) S431–S434.
[21] R. Hermann, H. Hermann, M. Calin, B. Büchner, J. Eckert, Elastic constants of single crystalline β-$Ti_{70}Nb_{30}$, Scripta Mater. 66 (2012) 198–201.
[22] J.C. Ho, E.W. Collings, Anomalous electrical resistivity in titanium-molybdenum alloys, Phys. Rev. B 6 (1972) 3727–3738.
[23] S.L. Ames, A.D. McQuillan, The resistivity-temperature-concentration relationships in the system niobium-titanium, Acta Metall. 2 (1954) 831–836.
[24] J.C. Williams, D. De Fontaine, N. Paton, The ω-phase as an example of an unusual shear transformation, Metall. Mater. Trans. B 4 (1973) 2701–2708.
[25] M. Ikeda, S. Komatsu, T. Sugimoto, K. Kamei, Temperature range of formation of athermal ω phase in quenched β Ti-Nb alloys, J. Jpn. Inst. Metals 52 (1988) 1206–1211.
[26] B.S. Hickman, The formation of omega phase in titanium and zirconium alloys: a review, J. Mater. Sci. 4 (1969) 554–563.
[27] S. Sikka, Y. Vohra, R. Chidambaram, Omega phase in materials, Prog. Mater. Sci. 27 (1982) 245–310.
[28] M. Tahara, H.Y. Kim, T. Inamura, H. Hosoda, S. Miyazaki, Role of interstitial atoms in the microstructure and non-linear elastic deformation behavior of Ti–Nb alloy, J. Alloys Compd. 577 (2013) S404–S407.
[29] D. Shindo, Y. Murakami, Advanced transmission electron microscopy study on premartensitic state of Ti_{50} $Ni_{48}Fe_2$, Sci. Technol. Adv. Mater. 1 (2000) 117–124.
[30] H. Bohm, Interpretation of X-ray scattering patterns due to periodic structural fluctuations. I. The case of transverse modulation of positional parameters in primitive lattices, Acta Crystallogr. A 31 (1975) 622–628.